Self-assembled 0D/2D nano carbon materials enabled smart and multifunctional cement-based composites

Sufen Dong[1], Linwei Li[2], Ashraf Ashour[3], Xufeng Dong[1], Baoguo Han[2, *]

[1] *School of Material Science and Engineering, Dalian University of Technology, Dalian, 116024 China*
[2] *School of Civil Engineering, Dalian University of Technology, Dalian, 116024 China*
[3] *Faculty of Engineering & Informatics, University of Bradford, Bradford, BD7 1DP, UK*
* Corresponding author: hithanbaoguo@163.com, hanbaoguo@dlut.edu.cn

Abstract: In this paper, two types of nano carbon materials including 0D nano carbon black and 2D graphene are assembled through electrostatic adsorption to develop smart cement-based composites. Owing to their excellent mechanical, electrical properties and synergistic effect, self-assembled 0D/2D nano carbon materials can form toughening and conductive networks in cement-based materials at low content level and without changing the preparation process of conventional cement-based materials, thus endowing cement-based materials with smart and multifunctional properties including high toughness, self-sensing property to stress/strain and damage, shielding/absorbing property to electromagnetic wave. The developed smart cement-based composites with self-assembled 0D/2D nano carbon materials have promising application in the fields of oil well cementing, structural health monitoring, and electromagnetic protection and anti-electromagnetic pollution. It can therefore conclude that electrostatic self-assembled 0D/2D nano carbon materials provide a simple preparation method and excellent composite effect for developing nano cement-based materials, which can be applied in large-scale infrastructures.

Key words: Cement-based composites; Self-assembled graphene/carbon black composite filler; Toughness; Self-sensing; Shielding/absorbing properties

1 Introduction

As the second most used resource after water, cement-based materials are commonly used to construct infrastructures such as buildings, highways, bridges and tunnels. However, cement-based material is a typical brittle material with low tensile strength, poor deformation performance and easy cracking characteristic, which has affected the safety, applicability and durability of civil engineering. Meanwhile, the absence of condition assessment tools and timely maintenance are also the chief reasons to the deterioration of concrete structures. Therefore, improving the toughness of cement-based materials and timely monitoring of infrastructure health are of great importance to reduce the life cycle cost of structures and save resource and energy [1]. The intelligent and multifunctional cement-based materials not only can be used as basic structural materials, but also can possess one or more types of intelligent or functional behaviors, such as self-sensing, self-healing, self-heating, self-cleaning, electromagnetic shielding/absorbing, energy harvesting, and light transmitting. This represents an innovative and sustainable development direction of cement-based materials. The smart and multifunction properties of cement-based materials can be achieved through introduction of functional components, composition design and modification of microstructures [2-8]. Of which, the incorporation of functional fillers is an effective approach to endow cement-based materials with different functions. The commonly used functional fillers include graphene [2], carbon black [3], carbon nanotube (CNT) [4, 5], nano carbon black (NCB) [6], carbon fiber [6], nano titanium dioxide [7] and nickel powder [8]. For example, Siad et al. [9] pointed out that incorporating CNTs with dosage of 0.5 wt% endows engineering cementitious composites with self-sensing and self-healing properties, simultaneously. Parvan et al. [10] concluded that at the curing ages of 180 days, cement mortar with 0.5-3 wt% NCBs

possesses excellent strain self-sensing property. Yıldırım et al. [11] found that compared to CNT, CF is a better conductive filler that can give concrete excellent self-sensing ability and have lower cost and easier mixability. Micheli et al. [12] pointed out that the electromagnetic wave shielding effectiveness for a 30 cm thick concrete wall with 3 wt% CNTs is greater than 50 dB. Meanwhile, the electromagnetic field attenuation is closely related to the wall thickness and CNT content.

As a typical 2D nano carbon material, graphene offers a possibility to develop tailored, high-performance, and multifunctional cement-based materials due to its remarkable mechanical, electrical, and thermal properties, excellent nanoscale effects, and low density [13-16]. Therefore, studies on the performance of cement-based materials with graphene fillers are of great value and can stimulate future development of civil construction technologies [17-30]. For example, Sun et al. [17] found that the incorporation of multi-layer graphenes can effectively improve the compressive strength and elastic modulus of cementitious composites and endow them with electrical conductivity, piezoresistive, electromagnetic interference shielding effectiveness and absorbing performance. Jin et al. [19] embedded graphene/cement composite into cement mortar to realize the real-time monitoring of chloride ion penetration in cement mortar. Hou et al. [20] pointed out that graphene has poor dispersibility in alkaline environments, leading to the reduction of hydration development and mechanical behavior of cement paste. Singh et al. [28] observed that incorporation of graphene oxide (30 wt%) along with an appropriate amount of ferrofluid in the cement matrix leads to a shielding effectiveness of 46 dB, which can be attributed to the strong polarizations and magnetic losses. Du et al. [29] concluded that the electrical resistivity of the cement mortar with graphene nanoplatelets decreases with the increase of graphene nanoplatelets content, and the percolation threshold is 2.4

vol%-3.6 vol%. They also pointed out that the insensitive property to moisture content of graphene nanoplatelet-infused mortar makes it a reliable damage-sensing material for infrastructure applications. It is worth noting that, physical dispersion measures or dispersant are usually needed in the preparation process of cement-based materials with graphene in order to improve the dispersibility and reduce the dosage of graphene [25-31]. This greatly increases the cost and complicates the production process of large infrastructures using cement-based materials with graphene. As a high cost-effective 0D nano carbon material, the incorporation of nano CB can also endow cement-based materials with electrical conductivity and self-sensing properties [32-34]. However, the mechanical behavior of cement-based materials is significantly weakened due to the addition of nano CB [35]. Parvan et al. [36] obtained the conclusion that with the increase of CB content, the amount of water required for the normal consistency increases and the final setting time of cement paste delays. They also point out that the dosage of CB can only be 0.5-1 wt% in order to maintain a considerable compressive strength compared to that of mortar without fillers.

In this paper, the 0D nano carbon black and 2D graphene are assembled through electrostatic adsorption to perform the synergistic combination effect which cannot get by adding alone or directly mixed nano carbon black and graphene. On the one hand, nano carbon black can improve the dispersibility of graphene without additional dispersion method and without changing the preparation process of cement-based materials [37, 38]. This is helpful for the mass production and energy reduction in the preparation of composites. On the other hand, 0D nano carbon black and 2D graphene can play short-range and long-range electrical conductivity, respectively, i.e. coupling effect, to give cement-based materials sensing property at low content level. In addition, the incorporation of graphene can offset the adverse effect of 0D nano carbon black on

the mechanical behavior of cement-based materials. Even, the 0D nano carbon black absorbed on the surface of graphene can enhance the micro-fiber effect of graphene [37, 38]. Owing to the excellent mechanical, electrical properties and size effect, the addition of self-assembled 0D/2D nano carbon materials, i.e. self-assembled graphene/nano carbon black (GCB) composite fillers, are potential to give cement-based materials with intelligence and multifunctionality. Hence, the GCB composite fillers were used to fabricate smart cement-based materials in this paper. The mechanical behavior, self-sensing, electromagnetic wave shielding and absorbing properties of cement-based materials with GCB composite fillers were investigated and the corresponding modification mechanisms were analyzed.

2 Experiment schemes

2.1 Raw materials and mix design

This study was performed on hardened cement pastes without aggregates, leading to that the raw materials included cement, water, water reducing agent and GCB composite fillers. The type of cement used was P·I 42.5 with density of 3.1 g/cm^3. The chemical position and properties of cement conform to the requirements of China's standard GB175-2007 <Common Portland Cement>. 3310E type polycarboxylate superplasticizer (produced by Sika, China) was used as water reducing agent and surfactant, simultaneously, to adjust the workability of mixture and improve the dispersion of GCB composite fillers [39, 40]. The SEM image of the GCB composite fillers was shown in Fig. 1 and their properties are listed in Table 1. GCB composite fillers were purchased from Chengdu (China) Organic Chemicals Co. Ltd. and the production process was as follows. In order to obtain uniform and stable GCB composite fillers, the cationic/nonionic compounded surfactant was used to make graphenes (with layers less than 3) have positive charge, and then the surface positively

charged graphenes and surface negatively charged carbon blacks (with specific surface area of 108 m^2/g) assemble through electrostatic adsorption. This means that the GCB composite fillers can produce the synergy effect of graphene and carbon black.

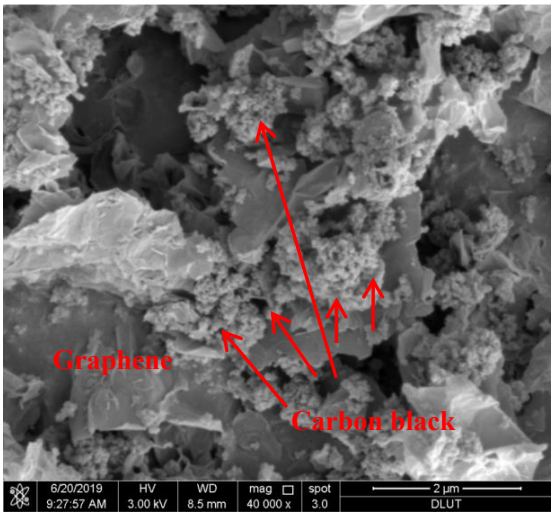

Fig. 1 SEM image of GCB composite fillers

Table 1 Main properties of graphene, carbon black and GCB composite fillers

Graphene content (wt%)	Graphene layers	Lateral size of graphene (µm)	Graphene purity (wt%)	Particle size of carbon black (nm)	GCB composite fillers		
					Specific surface area (m^2/g)	Specific resistance (Ω·cm)	Density (g/cm^3)
20	<3	8-15	98	20-25	121	0.233	2.12

Table 2 Composite mix details including mass and volume fractions of GCB fillers used

Specimens	Weight of raw materials for three samples, g				Water/cement ratio	GCB filler content (wt% of cement)	GCB filler content (vol% of composite)	Graphene content (vol% of composite)
	Cement	Water	GCB composite fillers	Water reducing agent				
GCB-0%	100	30	0	1.5	0.3	0	0	0
GCB-1.5%	100	30	1.5	1.5	0.3	1.5	1.15	0.23
GCB-3.0%	100	30	3.0	1.5	0.3	3.0	2.36	0.47
GCB-4.5%	100	30	4.5	1.5	0.3	4.5	3.35	0.67
GCB-6.0%	100	40	6.0	1.5	0.4	6.0	4.11	0.82
GCB-7.5%	100	40	7.5	1.5	0.4	7.0	5.08	1.02
GCB-9.0%	100	40	9.00	1.5	0.4	9.0	6.04	1.21

Table 2 presents the composites mix details including the mass and volume fractions of GCB used. In order to ensure the good workability of mixtures, the water cement ratio was increased to 0.4 when the dosage of GCB composite filler was larger than 4.5 wt% of cement. Although the dispersion becomes more difficult as the dosage of GCB composite filler increases [41], the dosage of water reducing agent with was fixed as 1.5 wt% of cement to avoid the influence of water in agent on properties of composites. The specimens were named after mass content of GCB composite fillers. For example, GCB-1.5% refers to cement-based materials with GCB composite fillers at mass content of 1.5%.

2.2 Specimens preparation

The mixing process of cement-based materials with GCB composite fillers was conducted as follows. Firstly, the weighed water, water reducing agent and GCB composite fillers were mixed for 30 seconds at a low speed of 1000±100 r/min using a mortar stirrer. Secondly, cement was added and the composites were mixed at the same low speed for 60 seconds, then, at high speed of 2000±100 r/min for 60 s. Thirdly, the mixture was poured into oiled molds (with size of 20 mm×20 mm×40 mm) in one-go, and then vibrated for 60 seconds to eliminate air bubbles. Lastly, two stainless steel gauze electrodes were embedded into the corresponding positions of specimens (10 mm measured from one side of specimens) to achieve the required connections for detecting the electrical and self-sensing properties of composites. After that, the specimens were vibrated for another 30 seconds in order to enhance the bond between electrodes and composites. Next, all specimens were kept in a standard curing chamber and then demoulded after 24 hours. Then, the specimens were cured in water at 20 °C for 28 days before testing.

160 *2.3 Measurements*

161 The electrical resistance of cement-based materials with GCB composite fillers was
162 tested at the curing ages of 3 days, 7 days, 14 days, 21 days and 28 days, respectively.
163 The two-electrode alternating current (AC) resistance was measured using an Agilent
164 U1733C Digital Multimeter at a frequency of 100 kHz in order to eliminate the effect
165 of polarization [42]. Meanwhile, the two-electrode direct current (DC) resistance was
166 measured by a Keithley 2100 digital multimeter. The electrical resistivity, ρ, is
167 calculated according to $\rho=RS/L$, where R is the electrical resistance, S is the cross-
168 sectional area and L is the distance between two electrodes. The electrochemical
169 impedance spectroscopy (EIS) of the composites was tested using electrochemical
170 analyzer. A frequency ranged from 10^{-2} Hz to 10^{5} Hz and a low-amplitude AC excitation
171 of 50 mV were used for EIS test in this study.

172 In order to study the self-sensing property of the composites, the cyclic compressive
173 loading was exerted on specimens with size of 20 mm×20 mm×40 mm under
174 displacement control arrangement and the loading rate was 0.4 mm/min. The maximum
175 value of the cyclic compressive loading is 8 kN (within an elastic regime). The strain
176 gauges were attached on the opposite sides of specimens along the loading direction
177 and perpendicular to the loading direction to test the longitudinal strain and transvers
178 strain, respectively. Dynamic strain indicator was employed to acquire the strain values.
179 At the same time, the two-electrode DC resistance measurement was carried out by
180 using Keithley 2100. The fractional change in electrical resistivity (FCR) is calculated
181 based on the equation of $FCR = 100\% \times (\rho_1 - \rho_0)/\rho_0$, where ρ_0 is the resistivity
182 without loading and ρ_1 is the resistivity under loading. The monotonic compressive
183 loading was exerted on the specimens with a loading rate of 1.2 mm/min after cyclic
184 compressive test. The longitudinal/transverse strain and two-electrode DC resistance

were, all, measured during the monotonic compression test. The average strain calculated from the measured two strain values was used to describe the relationship between FCR and cyclic/monotonic compressive strain/stress. The integration of compressive strain-stress curves was defined as compression work, representing the energy consumed during the process of compression.

The powder sample of the composites was prepared into annular specimen for electromagnetic wave property test, with 3.04 mm inner diameter and 7 mm outer diameter. The electromagnetic wave shielding effectiveness (SE) and reflectivity was calculated based on Eqs. (1) and (2) according to references [43, 44]. The test frequency range was 2-18 GHz. Meanwhile, the SEM images of GCB composite fillers and the composites were taken.

$$SE = 10lg(1 / |S_{12}|^2) = 10lg(1 / |S_{21}|^2) \quad (1)$$

where SE is the electromagnetic wave shielding effectiveness. On the basis of vector network method, S_{12} refers to the reverse transmission coefficient between surface 2 and surface 1 when the surface 2 is connected with a matched load, S_{21} refers to the reverse transmission coefficient between surface 1 and surface 2 when the surface 1 is connected with a matched load.

$$R = 20lg \frac{\left|\sqrt{\mu_r / \varepsilon_r}\tanh(j(2\pi fd / c)\sqrt{\mu_r / \varepsilon_r} - 1)\right|}{\left|\sqrt{\mu_r / \varepsilon_r}\tanh(j(2\pi fd / c)\sqrt{\mu_r / \varepsilon_r} + 1)\right|} \quad (2)$$

where R is the electromagnetic wave reflectivity, μ_r is the magnetic permeability, ε_r is the dielectric permittivity, h is the height of specimens, j is the imaginary unit, f is the frequency of the electromagnetic wave, d is the thickness of specimens, c is the transmission speed of the electromagnetic wave in air. There were three identical specimens for each composite mix. The strain-stress curves, EIS, strain-FCR curves,

stress-FCR curves, strain-stress-FCR curves, shielding effectiveness and reflectivity curves which is closest to the average one was selected to analyze the mechanical, self-sensing and electromagnetic wave characteristics of cement-based materials with GCB composite fillers. The average value of compressive strength, compressive work, AC electrical resistivity and DC electrical resistivity of three specimens for each composite was regarded as the final result. The sampling rate of stress, strain and FCR was 2 Hz.

3 Results and discussions

3.1 Compressive behavior

The compressive strain-stress curves of cement-based materials with GCB composite fillers are demonstrated in Fig. 2(a). It can be seen that the slope of strain-stress curves decreases with the increasing filler content. The peak stress of the composites displays a declining trend due to the incorporation of GCB composite fillers, while the peak strain of the composites increases from 5552 με to 8661 με. The strain-stress curve of cement-based materials without fillers shows a linear growth until peak stress, exhibiting typical brittleness material characteristic. However, the ascending stage of strain-stress curves of cement-based materials with GCB composite fillers consists of elastic and plastic regions. In addition, the plastic section prolongs with the increase of filler content, indicating that the addition of GCB composite fillers can effectively hinder the propagation of cracks and improve the deformation ability of cement-based materials, through bridging cracks and being pulled-out or pulled-off. Meanwhile, the elastic modulus can be calculated from the compressive stress to strain curves within the elastic limit where the stress is directly proportional to strain (40% of the maximum applied stress) according to the standards, i.e. ASTM C469. It can be found in Fig. 2(a) that the elastic modulus of GCB-0% with water-cement ratio of 0.3 is 23.2 GPa, which is comparable to the result of reference [17]. The elastic modulus decreases as the filler

content increase from 0% to 4.5%, and this can be attributed to the aggregation of GCB composite fillers, the reduction of mixture workability, and the increase of air content. When the water-cement ratio is 0.4, the decline amplitude of elastic modulus increases. The elastic modulus is decreased by 63.4% due to the addition of 9 wt% GCB composite fillers and the increase of water-cement ratio. In addition, the reduced elastic modulus allows the crack formations at lower loading level compared to control specimens, resulting in the prolong of the plastic stage on compressive stress-strain curves.

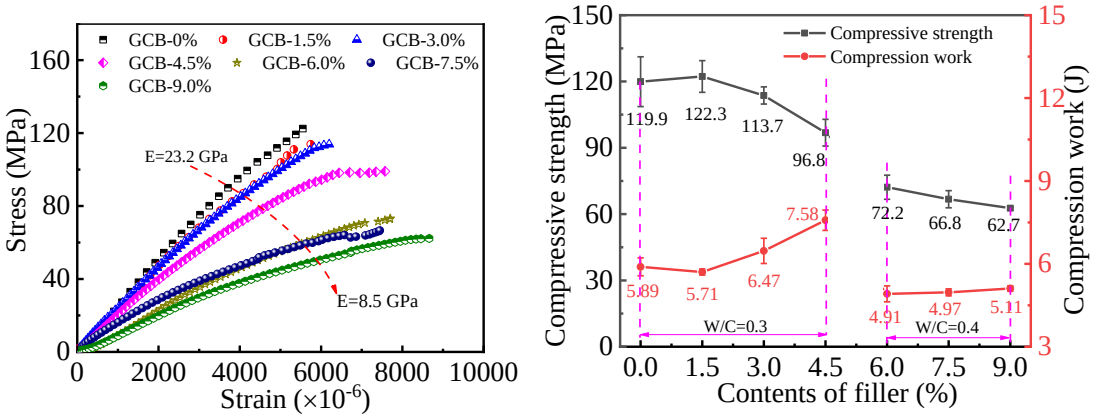

(a) Compressive strain-stress (b) Compressive strength and work

Fig. 2 Compressive behavior of cement-based materials with GCB composite fillers

Fig. 2(b) shows the compressive strength and compression work of cement-based materials with GCB composite fillers. It is clear that incorporating GCB composite fillers with content less than 3% has no adverse effect on the compressive strength of cement-based materials. The compressive strength lowers by 19.2% when the filler content is 4.5%. The reduced rate of compressive strength is 47.7% for GCB-9.0%, which can be ascribed to the increase of water to cement ratio and the adsorption effect of fillers. However, the compressive strength of GCB-4.5%, GCB-6.0%, GCB-7.5% and GCB-9.0% can still reach 96.8 MPa, 72.2 MPa, 66.8 MPa and 62.7 MPa, respectively. Meanwhile, the maximum reduction of compressive strength (47.7%) caused by the addition of GCB composite fillers is lower than that of elastic modulus

(63.3%, as shown in Fig. 2(a)), which is one sign of increased toughness and meets the requirements of oil well cement. Moreover, the compressive strength error bar of the composites with fillers is smaller than that of composites without fillers. This can be attributed to the good thermal conductivity of GCB composite fillers, leading to that the original temperature micro cracks can be reduced and the structural uniformity is increased. That is to say, the distribution of fillers is closely related to the property stability of composite. Therefore, the decrease of compressive strength error bar indicates the good dispersibility of GCB composite fillers from one aspect. Fig. 2(b) also demonstrates that at the same water to cement ratio, the compression work calculated by the strain-stress curve integration shows a growing tendency with the increase of GCB composite filler content. The increase of water-cement ratio significantly reduces the compression work of composites, resulting from the increase of macroscopic defects. The compression work of GCB-4.5% is 28.6% higher than that of GCB-0%, and the compression work of GCB-9% is only lowered by 13.3%. This can be attributed to the large longitudinal deformation of specimens. The compressive strength of GCB-9.0% (the corresponding volume fraction of graphene is 1.21%.) is 40.3% higher than that of Lu's research [45], while the elastic modulus is only improved by 28.9%, indicating that GCB-9.0% satisfies the requirement of oil well cement.

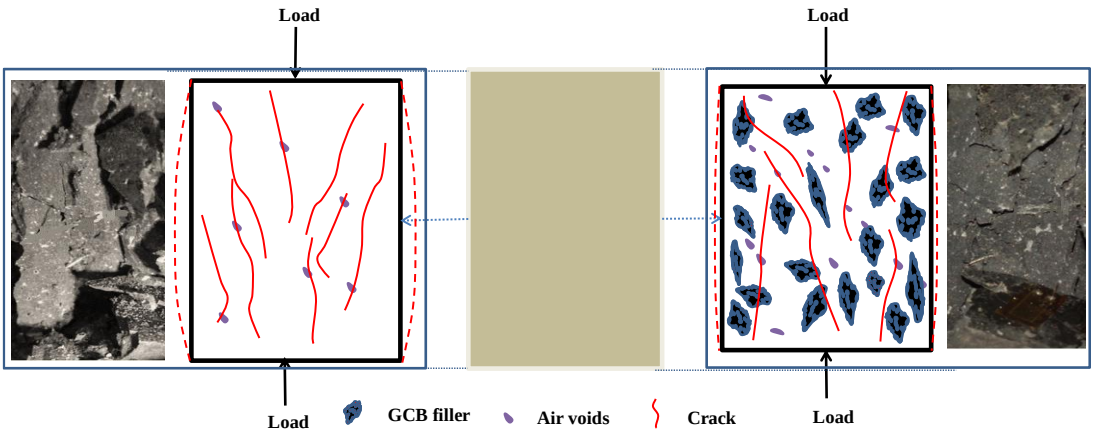

(a) Without GCB fillers (b) Specimens (c) With GCB fillers

Fig. 3 Compressive failure state of cement-based materials with GCB composite fillers

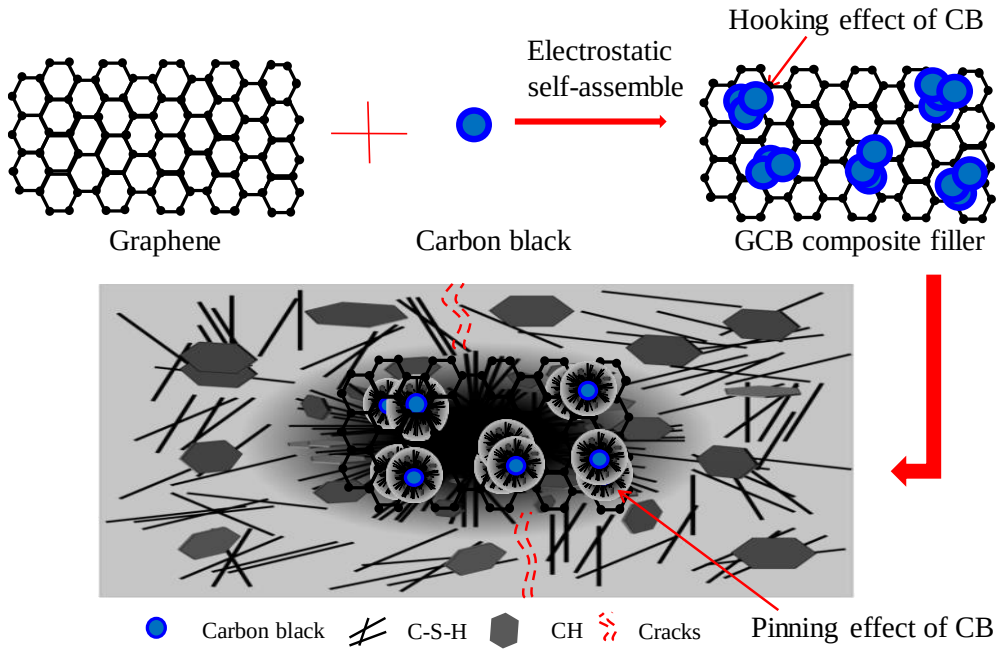

Hydration nucleation effect and micro fiber effect of GCB composite fillers in cement-based materials

Fig. 4 Toughening mechanisms of GCB composite fillers

The failure state of cement-based materials with GCB composite fillers under compression is demonstrated in Fig. 3. Because carbon black has strong water absorption [46, 47], the fluidity of the composites becomes worse with the increasing fillers. This leads to an increase of the air content and macroscopic defects. Therefore, the compressive strength and elastic modulus decreases, too. However, it should be noted that the longitudinal strain of the composites and compression work increases due to the incorporation of fillers. It can be attributed to that this kind of electrostatic self-assembled GCB filler can play hydration nucleation effect and micro fiber effect in cement-based materials [48, 49], simultaneously, as shown in Figs. 4 and 5. Fig. 5 demonstrates that the micro fiber effect of GCB composite fillers can reduce original cracks and inhibit the initiation and propagation of existing cracks. Meanwhile, the GCB composite fillers in the margin zone of specimens have lateral restraint effect and increase longitudinal deformation. It is worth noting that the self-assembled CBs on

285 graphene act as hooking units and they are also hydration nucleus in cement-based
286 materials [49], also as demonstrated in Figs. 4 and 5. The hooking function of CBs
287 endows graphene with characteristic like special-shaped steel fiber or ribbed bar, i.e.,
288 the addition of graphene with CBs hooking units can significantly improve the after-
289 cracking properties of cement-based materials. In other words, the CBs coated with
290 hydration products endow graphene self-pinning effect, effectively inhibiting the
291 debonding and being pulled-out of graphene. This is consistent with the conclusion that
292 the non-linear stage on the compressive strain-stress curves of cement-based
293 composites increases with the increase of filler content. The characteristics of high
294 compressive strength, low elastic modulus, large longitudinal strain and high
295 compression work of the composites provide feasibility for its use in oil well cementing.

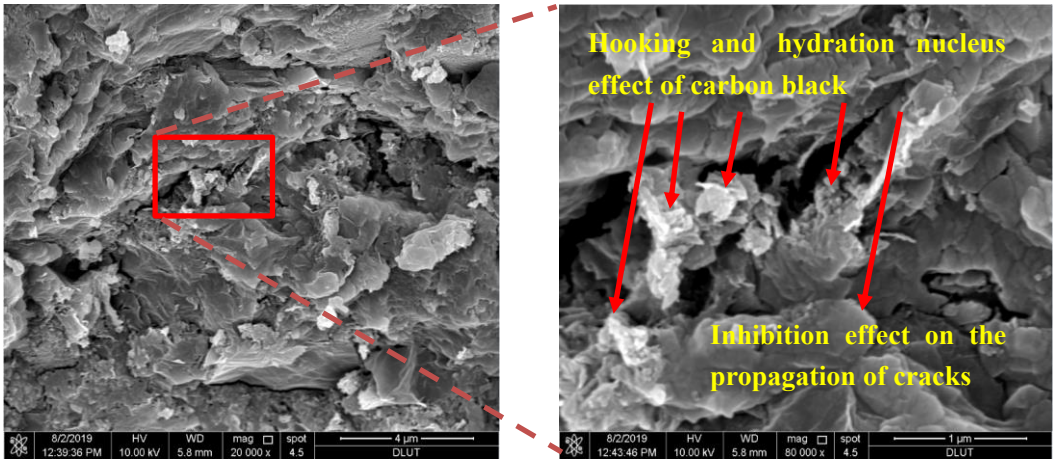

Fig. 5 The inhibition effect of GCB composite fillers on the propagation of cracks

296

297 *3.2 Electrical resistivity and self-sensing property*

298 3.2.1 Electrical resistivity

299 Fig. 6 shows the DC and AC electrical resistivity of cement-based materials with
300 GCB composite fillers. Fig. 6(a) indicates that when the content of fillers is smaller
301 than 4.5%, the DC electrical resistivity of the composites decreases with the increased
302 filler content and it also increases with the increase of curing ages. As the content of
303 fillers increases from 0% to 4.5%, the DC electrical resistivity of the composites at the

curing ages of 28 d can lower from 35×10^4 Ω·cm to 0.9×10^4 Ω·cm. The increase of water-cement ratio also leads to the decrease of electrical resistivity. When the water-cement ratio is 0.4, the DC electrical resistivity of GCB-6.0%, GCB-7.5% and GCB-9.0% is 1932 Ω·cm, 510 Ω·cm and 182 Ω·cm, respectively, representing that GCB composite fillers have been overlapped to form conductive network. That is to say, the DC electrical resistivity of cement-based martials can be reduced by three orders of magnitudes under the combination effect of GCB composite fillers and water-cement ratio. The two-electrode DC electrical resistivity of GCB-9.0% is two orders of magnitudes lower than that of cement-based composites with 10 wt% MLGs [17], indicating the synergistic effect of GCB composite fillers. Meanwhile, this value is comparable to that of cement paste with water-cement ratio of 0.4 and 20 wt.% carbon black [3], and the four-electrode electrical resistivity of cement paste with 1.0 wt% MWCNTs [50].

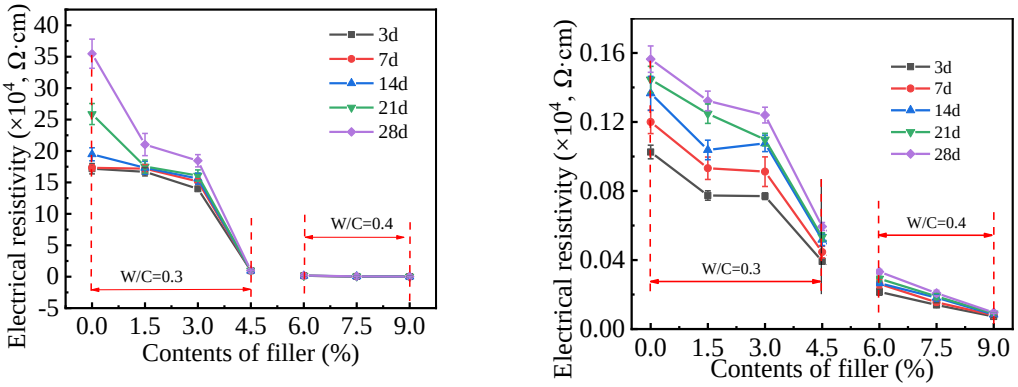

(a) DC electrical resistivity (b) AC electrical resistivity

Fig. 6 Electrical resistivity of cement-based materials with GCB composite fillers

As shown in Fig. 6(b), the AC electrical resistivity of the composites has the same change rule with that of DC electrical resistivity. When the filler content is 1.5%, the conductive pathway is formed mainly by cement matrix. The AC electrical resistivity of GCB-4.5% is 534 Ω·cm, reduced by one order of magnitude compared to that of GCB-0%, indicating that the fillers can form widely distributed conductive network in

cement-based materials. As the filler content increases from 6.0% to 9.0%, the electrical resistivity of composites decreases from 292 Ω·cm to 90 Ω·cm, two orders of magnitudes lower than that of GCB-0%. The relative reduction between GCB-4.5% and GCB-6.0% mainly comes from the effect of water-cement ratio. Contrast analysis between Fig. 6(a) and 6(b) manifests that the AC electrical resistivity of the composites is four orders of magnitudes lower than that of DC electrical resistivity due to the polarization effect. The AC electrical resistivity of GCB-9.0% is one order of magnitude lower than that of cement-based composites with 9 wt% MLGs [17].

3.2.2 Electrochemical impedance spectroscopy (EIS)

The EIS of cement-based materials with GCB composite fillers can be drawn in Nyquist plot, as shown in Fig. 7. It can be seen from Fig. 7 that with the frequency in each plot decreasing from left to right, the location, time parameter and topological structure of EIS vary with filler content. The deviation between the AC resistivity of composites and the values of EIS starting points (at the frequency of 100 kHz) is less than 15%, indicating the data validity and repeatability. The various stages of EIS can be represented by electrical basic equivalent element (such as resistance, capacitance and constant phase angle) and composite equivalent element (e.g. the series or parallel of resistance and capacitance) [51-54], and then the equivalent circuit can be plotted to qualitatively analyze the electric kinetic process of the composites, as demonstrated in Fig. 8. Fig. 7(a) shows that for GCB-0%, the EIS includes a small arc and an oblique line in the first quadrant, representing the conductive pathway in the composites mainly depends on the charge diffusion impedance of cement matrix and the electrodes' response due to ions from the pore solution. The corresponding equivalent circuit can be plotted in Fig. 8(a). The charge diffusion process through cement matrix and electrode is expressed by the parallel of resistance and constant phase angle. R_1

348 represents the charge diffusion impedance of cement matrix, R_2 indicates the contact
349 impedance between electrode and cement matrix, Q_1 is the double layer capacitance
350 formed by hydration C-S-H gels, and Q_2 is the interfacial double layer capacitance
351 between electrode and cement matrix. The EIS and the corresponding equivalent circuit
352 of GCB-1.5% are similar to that of GCB-0%. When the filler content is 4.5%, the EIS
353 of the composites consists of two semi-arcs (as shown in Fig. 7(b)), the conductive
354 pathway of which is determined by GCB composite fillers and cement matrix together.
355 The topological structure of EIS for GCB-3.0% is the same to that for GCB-4.5%. The
356 appearance of the first flat semi-arc can be attributed to the formation of capacitor plate
357 caused by fillers and pore solution. The corresponding composite equivalent element
358 can be expressed by the parallel of resistance, capacitance and the series of resistance
359 and constant phase angle, as shown in Fig. 8(b). The second semi-arc of EIS is caused
360 by the charge diffusion process at the position of electrodes. In Fig. 8(b), R_3 represents
361 the overlapped resistance formed by GCB composite fillers, Q_3 is the double layer
362 capacitance between GCB composite fillers and cement matrix. As plotted in Figs. 7(c)
363 and (d), the EIS of GCB-6.0%and GCB-9.0% has the same topological structure and
364 they are all composed of a quadrant arc and a semi-arc together. GCB-7.5% possess the
365 same EIS topological structure as GCB-6.0% and GCB-9.0%. The conductive pathway
366 in these specimens is mainly constituted of overlapped GCB composite fillers, and this
367 is hardly affected by water-cement ratio. Fig. 8(c) shows that the capacitance plate
368 element on the surface of fillers can be used to represent the quadrant arc part of EIS,
369 and the formation of semi-arc part of EIS is ascribed to the charge diffusion on the
370 surface of electrodes which is expressed by the parallel of resistance and constant phase
371 angle. ZsimpWin software is used to fit and analyze the conductive pathway model of
372 cement-based materials with GCB composite fillers, and the fitting results are shown

in Fig. 6. The value of Chi-squared which characterizes the fit degree is less than 1.21×10^{-3}, agreeing well with the measured results of EIS, and the selected equivalent circuits are reasonable for describing EIS of the composites.

It can be concluded that the fillers can disperse well in cement-based materials and is more likely to form conductive network. This can be attributed to the following: 1) the electrical resistivity of GCB composite filler is only 0.233 Ω·cm; 2) the size of composite filler is larger than that of graphene alone or carbon black alone; 3) the graphene in GCB composite fillers plays the role of long-range conduction and the carbon black possesses short-range conduction effect.

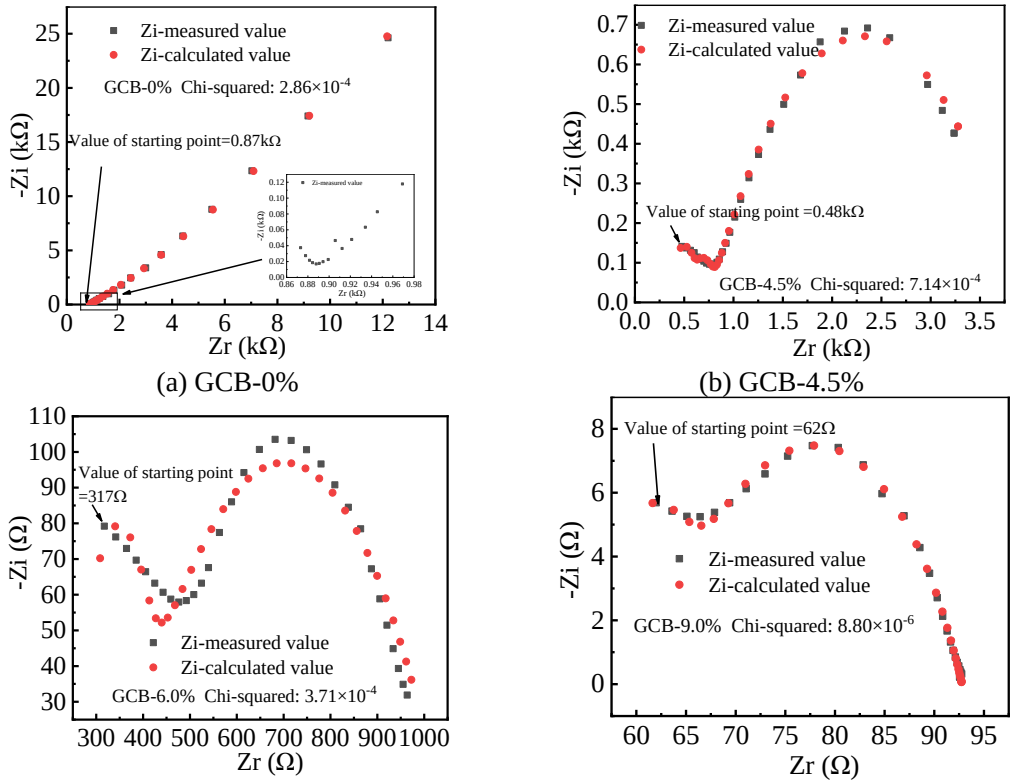

(a) GCB-0% (b) GCB-4.5%

(c) GCB-6.0% (d) GCB-9.0%

Fig. 7 EIS of cement-based materials with GCB composite fillers

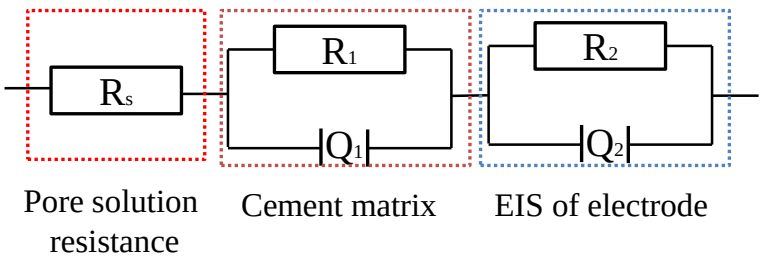

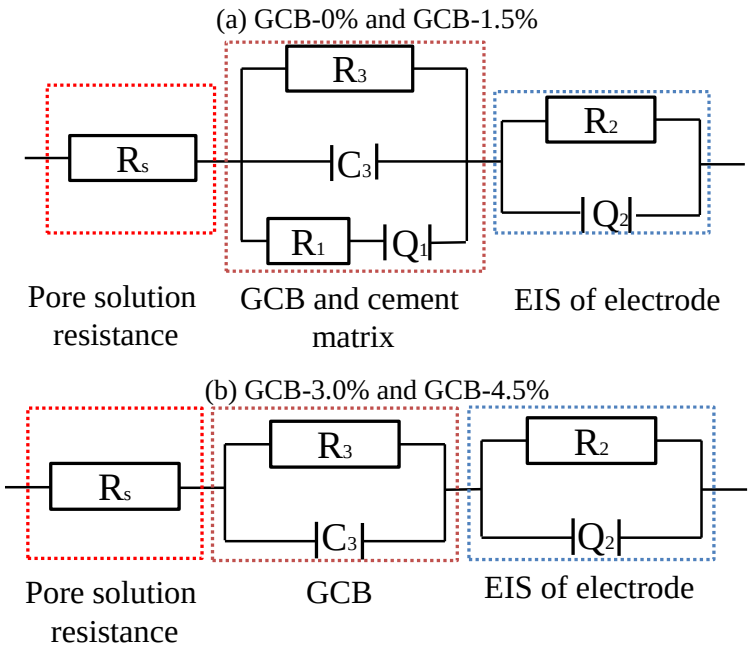

(c) GCB-6.0%, GCB-7.5% and GCB-9.0%

Fig. 8 The equivalent circuit of cement-based materials with GCB composite fillers (R_1 represents the charge diffusion impedance of cement matrix, R_2 indicates the contact impedance between electrode and cement matrix, and R_3 represents the overlapped resistance formed by GCB composite fillers. Q_1, Q_2 and Q_3 is the double layer capacitance formed by hydration C-S-H gels, the interfacial double layer capacitance between electrode and cement matrix and the interfacial double layer capacitance between GCB composite fillers and cement matrix, respectively.)

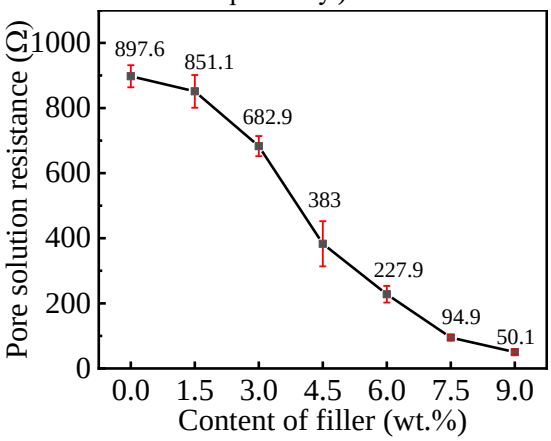

Fig. 9 Pore solution resistance of cement-based materials with GCB composite fillers

The pore solution resistance R_s can be obtained by ZsimpWin software fitting. and the value of R_s is an inverse function of porosity and pore solution concentration. As shown in Fig. 9, the pore solution resistance R_s decreases with the increasing filler content. This can be attributed to that the micro pore amount in the composites increases due to the incorporation of GCB composite fillers. Meanwhile, the ionic adsorption

happens on the surface of CB, causing the enhancement of ionic concentration in pore solution. The change rule of pore solution resistance with filler content is the same with that of AC electrical resistivity. When the water-cement ratio is 0.3, the pore solution resistance decreases from 682.9 Ω to 383 Ω as the dosage of GCB composite filler increases from 3.0% to 4.5%. In contrast, the pore solution resistance of GCB-6.0% is 227.9 Ω, only decreased by 40.5% in the combination effect of the increase of filler content and water-cement ratio. The above analyses indicate that the conductive pathway has been well established when GCB composite fillers content is 4.5%. Since conductive pathways formed by the connection of fillers are continuously established, the pore solution resistance is insignificantly influenced by cement matrix.

3.2.3 Self-sensing properties

1) Under cyclic compressive loading

Experimental results show that GCB-4.5% has the best stable, repeatable and sensitive self-sensing properties compared to other composites as the content of filler for GCB-4.5% is in the percolation threshold zone. Therefore, the time history relationships of stress/strain and FCR for GCB-4.5% are established, as demonstrated in Fig. 10. The cyclic stress amplitude is set at 20 MPa which is less than 1/3 of the minimum compressive strength of the composites to ensure the deformation of specimens within the elastic regime. It can be seen from Fig. 10 that the FCR of GCB-4.5% decreases upon loading and increases upon unloading, which indicates that the composite has stable and reversible piezoresistive response. The function relationships between strain/stress and FCR of GCB-4.5% are shown in Fig. 11. The quadratic polynomial is used to fit the relationship between strain/stress and FCR, and the goodness of fit is larger than 0.99, confirming again that the composite has stable piezoresistive response under cyclic compressive loading.

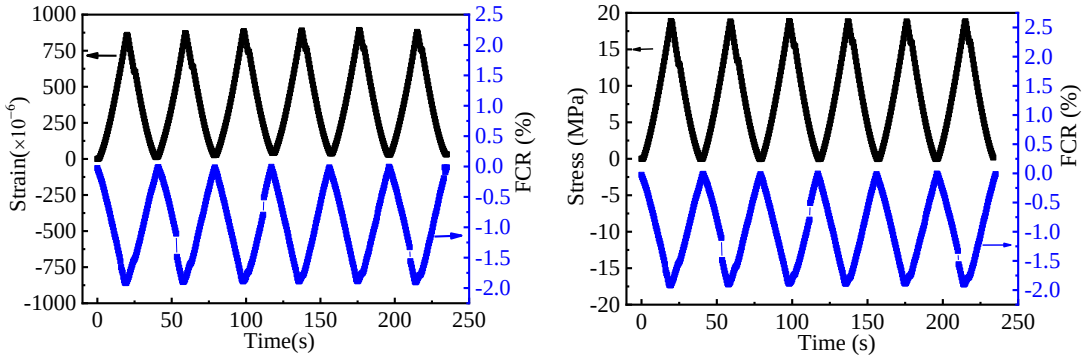

(a) Strain-FCR (b) Stress-FCR

Fig. 10 Time history relationships between FCR and cyclic stress/strain of GCB-4.5%

414

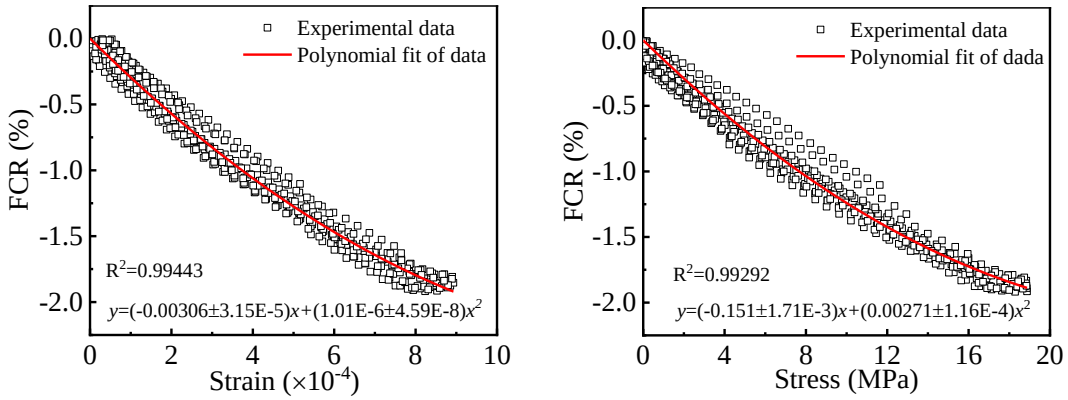

(a) Strain-FCR (b) Stress-FCR

Fig. 11 Function relationships of strain/stress and FCR of GCB-4.5% under cyclic compressive loading

415

416 The strain sensitivity (SAS) of cement-based materials with GCB composite fillers

417 can be calculated by the following Eq. (1).

418 $$SAS = \frac{FCR_{max}}{\varepsilon} \quad (3)$$

419 where SAS is strain sensitivity, FCR_{max} is the maximum FCR during the process of

420 compressive loading, ε is the compressive longitudinal strain corresponding to the

421 maximum FCR. The SAS of composites under 6 times of cyclic compressive loading

422 are plotted in Fig. 12. Through comparable analysis, it is found that the change rule of

423 strain sensitivity of the composites with the content of fillers has a similar tendency

424 with EIS. The FCR under cyclic compression loading is 0.2%, 0.2%, 0.3%, 1.9%, 2.4%,

425 2.8%, 3.0% for GCB-0%, GCB-1.5%, GCB-3.0%, GCB-4.5%, GCB-6.0%, GCB-7.5%

and GCB-9.0%, respectively. Meanwhile, the increase of water-cement ratio reduces the compressive strength and elastic modulus of composites, leading to the increase of deformation under the same loading level. The corresponding values of cyclic compressive strain are 750 ($\times10^{-6}$), 800 ($\times10^{-6}$), 800 ($\times10^{-6}$), 1000 ($\times10^{-6}$), 1300 ($\times10^{-6}$), 1600 ($\times10^{-6}$) and 1900 ($\times10^{-6}$), respectively. It is clear from Fig. 12 that GCB-1.5% has nearly the same strain sensitivity value as GCB-0%, which is caused by the elastic deformation of the specimens. This also means that GCB-1.5% has no self-sensing property. When the content of fillers is 3.0%, the strain sensitivity is only increased by 44.2%. When the content of GCB composite fillers is 4.5%, the strain is only increased by 33.3%, in contrast, the fractional change in electrical resistivity is improved by 8.5 times. This means that the strain sensitivity of GCB-4.5% is 630.8% higher than that of GCB-0%. For the composites with filler content larger than 4.5%, the strain sensitivity of the composites decreases with the increasing filler content. Although the elastic deformation of the specimens is enlarged due to the increase of water to cement ratio, it has no beneficial effect on the strain sensitivity, indicating that conductive pathway has been formed in GCB-4.5%.

The strain sensitivity of the composites can be attributed to the following factors. First, the specimens have elastic deformation and the resistance of GCB composite fillers will change under cyclic compressive loading. Second, the distance between fillers becomes smaller under compression, which connects adjacent fillers or improves the chance of tunneling effect. Third, the resistance between filler and cement matrix interface decreases with the increasing compressive loading. It should be noted that the change of the distance between fillers is the main factor among them. When the filler content is less than 3.0%, the distance between fillers is too far away to overlap with each other or even has no tunneling effect. Therefore, GCB-1.5% and GCB-3.0% have

high electrical resistivity and low piezoresistive property. As the filler content is 4.5%, they can be evenly distributed in cement matrix and are very close together. As a result, the electrical resistivity of GCB-4.5% is lowered by two orders of magnitude. When subjected to compression, the distance between fillers is reduced and the chance of tunneling conductive effect increases. For GCB-6.0%, GCB-7.5% and GCB-9.0%, the fillers in the composites have overlapped with each other. Meanwhile, the resistance of the overlapped fillers varies little under compression. Furthermore, the increase of water-cement ratio for GCB-6.0%, GCB-7.5% and GCB-9.0% improves the integrity of conductive pathway by providing pore solution and ionic conductance. This is why the strain sensitivity of these composites is not as high as that of GCB-4.5%. The strain sensitivity of the cement-based materials with 4.5 wt% GCB composite fillers, i.e. 0.69 vol% graphene, is 280.0% higher than that of cement-based materials with 2 vol% multi-layer graphenes (MLGs) [17]. Meanwhile, cement composites with carbon black less than 7 wt% have no piezoresistive properties in the research of Monteiro et al. [33], indicating that GCB composite filler has better dispersion property than carbon black.

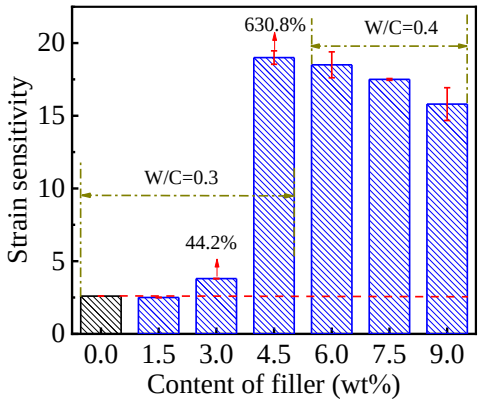

Fig. 12 Strain sensitivity of cement-based materials with GCB composite fillers under 6 times of cyclic compressive loading

2) Under monotonic compressive loading

The strain-stress and strain-FCR curves of cement-based materials with GCB composite fillers under monotonic compressive loading are shown in Fig. 13. It is clear

that the curves of strain-stress and strain-FCR possess the same trend. When the filler content is less than 3.0%, the absolute value of FCR first exhibits linear growth and then suddenly increases with the increasing compressive stress/strain, the maximum absolute value of which is 3.7%, 5.7% and 8.4% for GCB-0%, GCB-1.5% and GCB-3.0%, respectively, as shown in Fig. 13(a). This can be mainly attributed to the variation of specimen deformation under loading. For GCB-4.5%, the maximum absolute value of FCR reaches 16.1%, which is caused by the change of filler conductive pathway and specimen deformation together. Fig. 13(b) illustrates that the curves of stress-strain and strain-FCR of GCB-6.0%, GCB-7.5% and GCB-9.0% all include elastic and plastic two stages, and the plastic stages prolong with the filler content increases. The maximum absolute value of FCR for GCB-6.0%, GCB-7.5% and GCB-9.0% is 12.0%, 8.4% and 9.5%, respectively. Meanwhile, the maximum strain of these composites is 7703 με, 7446 με and 8662 με respectively, indicating that the specimen deformation plays an important role on the FCR value. The FCR of the composites first increases and then decreases with the increase of filler content.

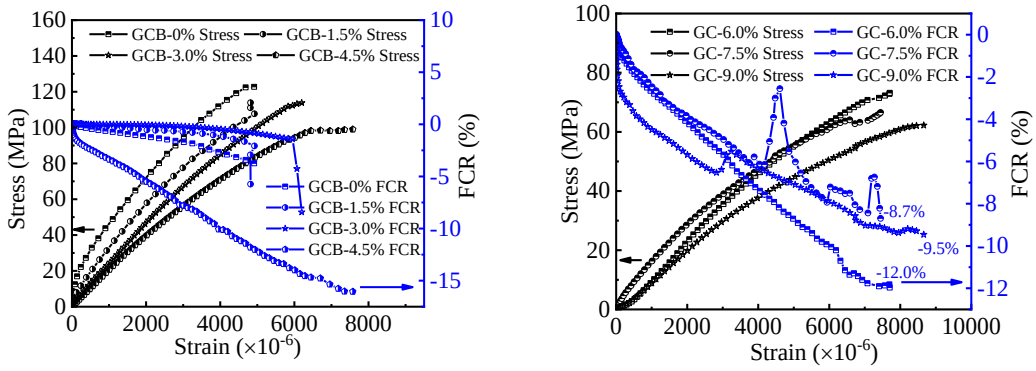

(a) Strain-FCR (b) Stress-FCR

Fig. 13 Compressive stress/strain and FCR of cement-based materials with GCB composite fillers under monotonic compressive loading

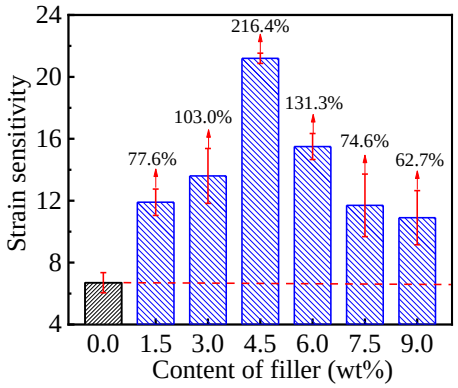

Fig. 14 Strain sensitivity of cement-based materials with GCB composite fillers under monotonic compressive loading

The strain sensitivity of cement-based materials with GCB composite fillers under monotonic compressive loading is plotted in Fig. 14. It can be seen from Fig. 14 that the strain sensitivity possesses the same change trend with the FCR, which is also closely related to the overlap state of GCB composite fillers and specimen deformation of the composites. The strain sensitivity first increases and then decreases with the increase of filler content. The change rule of strain sensitivity under monotonic compressive loading is consistent with that under cyclic compressive loading. when the dosage of fillers is larger than 4.5%, the fractional change in electrical resistivity does not increase with the deformation increasing, again indicating that the conductive pathway in composites of GCB-6.0%, GCB-7.5% and GCB-9.0% is determined by the overlapped GCB composite fillers and is slightly influenced by cement matrix. Therefore, the increase of water-cement ratio has no benefit on the strain sensitivity of composites. The maximum strain sensitivity of GCB-4.5% is 21.2, which is comparable to that of concrete with 10 wt% carbon black (with strain sensitivity of 24) [33].

3.3 Electromagnetic wave shielding and absorbing property

3.3.1 Electromagnetic wave shielding property

The shielding effectiveness (SE) of cement-based materials with GCB composite fillers in the frequency of 2-18 GHz are exhibited in Fig. 15. As can be seen in Fig. 15,

the incorporation of GCB composite fillers can significantly improve the SE of cement-based materials. When the frequency is lower than 14.4 GHz, the SE of the composites increases with the filler content increasing. The SE of GCB-0% and GCB-1.5% first increases and then remain stable, in contrast, the SE of other composites first increases and then decreases with the increasing frequency. Meanwhile, the SE decrease rate at the frequency of larger than 9.6 GHz presents a decreasing tendency due to the increase of water-cement ratio of composites. In addition, the frequency corresponding to the maximum value of SE decreases with the increase of filler content. At the frequency of 2 GHz, the SE of GCB-0% is only 0.30 dB which increases to 1.04 dB, 1.36 dB, 2.01 dB and 2.43 dB when the GCB filler content is 4.5%, 6.0%, 7.5% and 9.0%, respectively. When the frequency is 9.6 GHz, the SE of GCB-9.0% reaches 6.55 dB and is 2.0 times of that of GCB-0% at the combined effect of GCB composite fillers and the increased water-cement ratio. The SE of the cement-based materials with 9.0 wt% GCB composite fillers, i.e. 1.21 vol% graphene, is comparable to that of cement-based materials with 1 vol% MLGs (6.88 dB) [17]. Meanwhile, it is 31.8% and 19.0% higher than that of composites with 2.4 vol% short-carbon nanotube/nano carbon black(S-CNT/NCB) and 1.41 vol% long-carbon nanotube/nano carbon black (L-CNT/NCB) [49]. However, it is worth noting that although the SE of composites has not yet met the requirements (larger than 10 dB) of industrial and commercial application, the use of cement-based materials with GCB composite fillers can reduce the construction cost of infrastructures with electromagnetic wave shielding requirements.

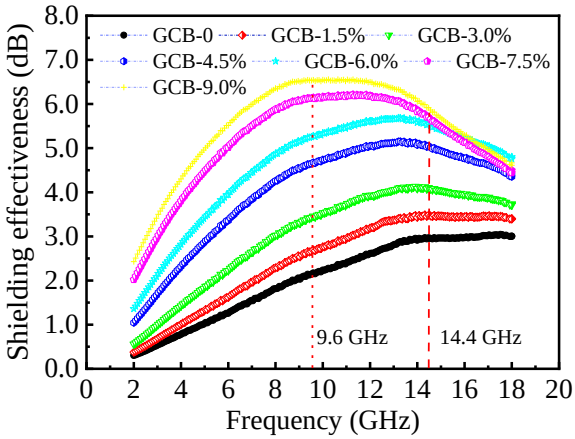

Fig. 15 SE of cement-based materials with GCB composite fillers in the frequency of 2 to 18 GHz

527

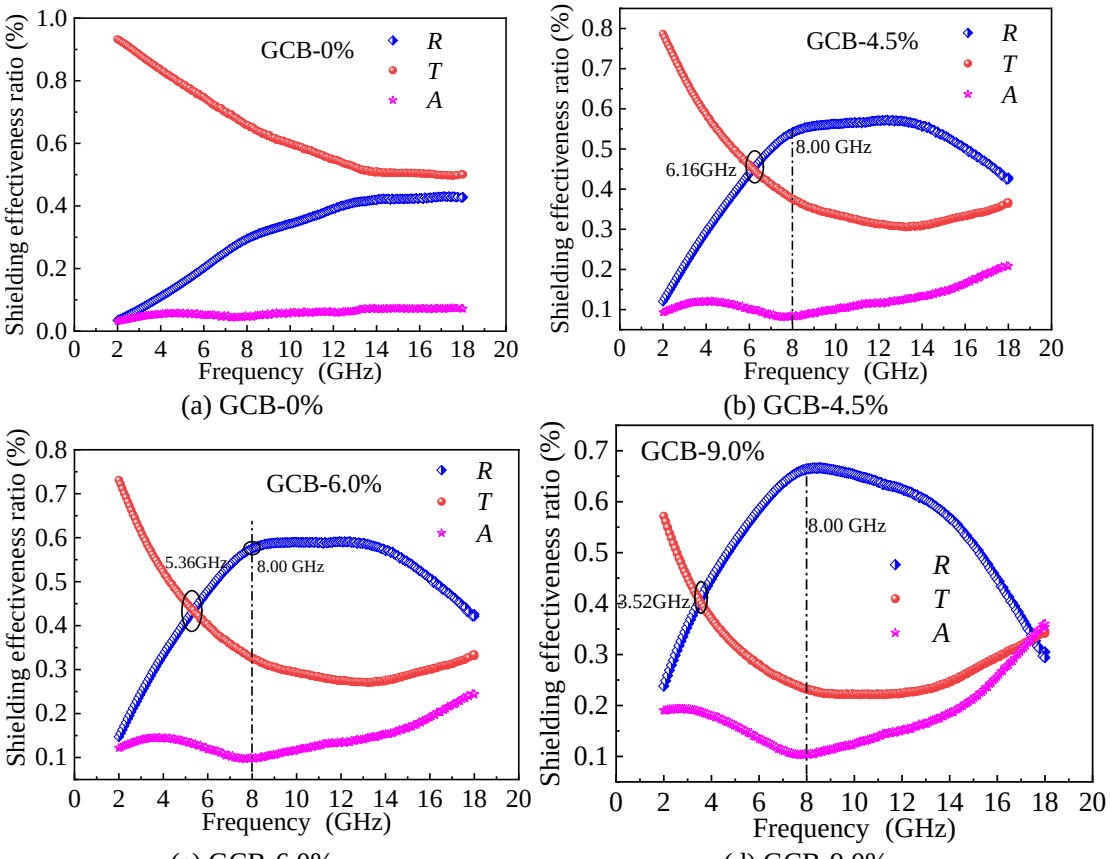

Fig. 16 The proportion of reflection loss (R), transmission loss (T) and absorption loss (A) of cement-based materials with GCB composite fillers in 2-18 GHz

528

529 The shielding mechanisms can be revealed through parameters analysis including

530 reflection loss, transmission loss and absorption loss. The proportion of reflection loss,

531 transmission loss and absorption loss in the SE of the composites are shown in Fig. 16.

532 For GCB-0%, the proportion of transmission loss is more than 50% and the proportion

533 of reflection loss is less than 40%, while the proportion of absorption loss is basically

zero in the frequency of 2-18 GHz. Meanwhile, the proportion of transmission loss decreases and the proportion of reflection loss increases with the frequency increasing. Due to the addition of GCB composite fillers, the proportion of reflection loss is higher than that of transmission loss when the frequency is larger than a certain value. The corresponding value of frequency is 12.50 GHz, 8.56 GHz, 6.16 GHz, 5.36 GHz, 4.00 GHz and 3.52 GHz for GCB-0%, GCB-1.5%, GCB-3.0%, GCB-4.5%, GCB-6.0%, GCB-7.5% and GCB-9.0%, respectively. This suggests that the incorporation of GCB composite fillers endows cement-based materials with high reflectivity ability especially to low frequency electromagnetic wave. Fig. 16 also shows that when the filler content is larger than 4.5%, the proportion of reflection loss first increases and then decreases while the proportion of transmission loss first decreases and then increases with the increase of frequency. In addition, the proportion of absorption loss exhibits linear growth with frequency as the frequency is larger than 8 GHz. This indicates that in X (8-12.5 GHz) and Ku (12.5-18 GHz) wave band, the absorption ability to electromagnetic wave of the composites is improved by the inclusion of GCB composite fillers. The proportion of absorption loss for GCB-9.0% is as high as 35% at the frequency of 17-18 GHz, which can be attributed to high conductivity of the composites.

3.3.2 Electromagnetic wave absorbing property

The reflectivity of cement-based materials with GCB composite fillers in the thickness of 10 mm and 20 mm at the frequency of 2-18 GHz is demonstrated in Fig. 17. The frequency range includes S (2-4 GHz), C (4-8 GHz), X (8-12.5 GHz) and Ku (12.5-18 GHz) wave band. It can be seen from Fig. 17(a) that the minimum reflectivity values of the composites in the thickness of 10 mm move to low frequency and their absolute values increase due to the incorporation of GCB composite fillers. At the

frequency of S (2-4 GHz) wave band, the absolute value of reflectivity increases with increased filler content. When the filler content is 9.0%, the maximum absolute value of reflectivity of the composites reaches 19.6 dB, which is 7.9 times of that of the composites without fillers. In the frequency range of C (4-8 GHz) wave band, the maximum absolute value of reflectivity of the composites first increases and then decreases with the increase of filler content. The composite with 6.0% of fillers presents the maximum absolute value of reflectivity of 28.7 dB, which is improved by 13.7 times compared to that of GCB-0%. This is comparable to the reflectivity of cement-based materials with 9 vol% of MLGs (29.8 dB) at the frequency of 7.6 GHz [17]. The composites of GCB-4.5%, GCB-6.0%, GCB-7.5% and GCB-9.0% possess peak reflectivity at the frequency range of X (8-12.5 GHz) wave band, and the absolute value of the peak reflectivity decreases with the increasing filler content. The maximum absolute value of reflectivity of GCB-4.5% is 14.1 dB, which is 1.8 times of that of GCB-0%. The absolute value of peak reflectivity of GCB-0%, GCB-1.5% and GCB-3.0% is 11.8 dB, 14.4 dB and 22.3 dB, respectively, at the frequency range of Ku (12.5-18 GHz) wave band. The above analysis shows that the content of fillers which can endow the best electromagnetic wave absorbing performance to cement-based materials decreases with the increase of wave frequency. That is to say, the composite with high electrical resistivity has good electromagnetic wave absorbing performance in the high frequency band, while the high conductive composites can effectively absorb low frequency electromagnetic wave. Therefore, the increase of water-cement ratio is conductive to the improvement of electromagnetic wave absorbing property of composites at low frequency. It is because the penetrating power of high frequency electromagnetic wave is better than that of low frequency electromagnetic wave, and magneto electric conversion is an effective way to consume low frequency

electromagnetic wave.

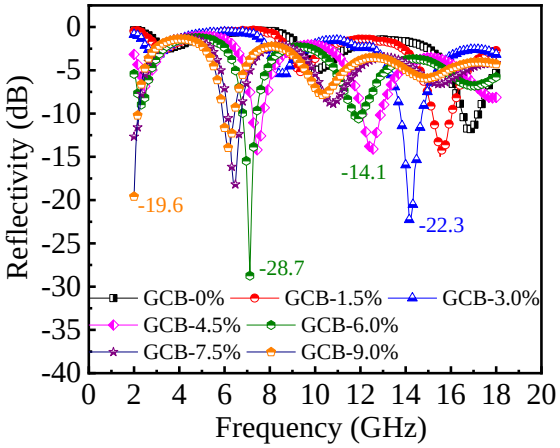

(a) In thickness of 10 mm

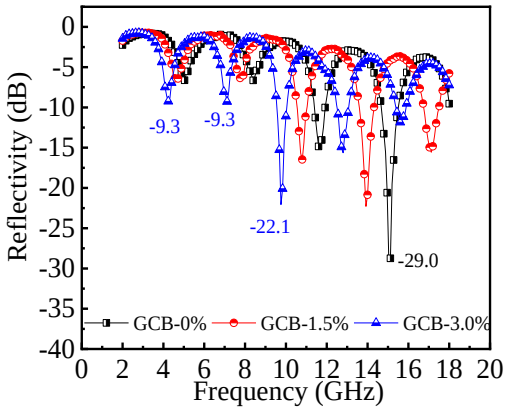

(b) In thickness of 20 mm

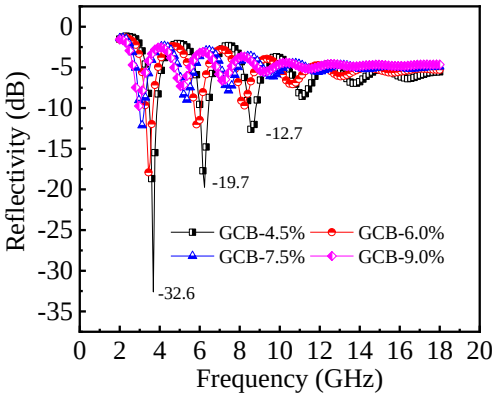

(c) In thickness of 20 mm

Fig. 17 The reflectivity of cement-based materials with GCB composite fillers in frequency of 2-18 GHz

Fig. 17(b) and (c) show the reflectivity of cement-based materials with GCB composite fillers in thickness of 20 mm at frequency range of 2-18 GHz. It can be found that the incorporation of GCB composite fillers lowers the electromagnetic wave absorbing performance of the composites at the frequency range of Ku (12.5-18 GHz) wave band, especially when the filler content is larger than 4.5%. At the frequency of S (2-4 GHz) and C (4-8 GHz) wave band, the composites with 4.5% fillers exhibit the best electromagnetic wave absorbing property and the maximum absolute value of reflectivity can reach 32.6 dB and 19.7 dB, respectively. These are 4.9 times and 3.0 times of that of composites without fillers. At the frequency of X (8-12.5 GHz) wave band, the GCB-3.0% displays the best electromagnetic wave absorbing performance

and the maximum absolute value of reflectivity is 22.1 dB. The cement-based materials with GCB composite fillers in 10 mm thickness perform better in the term of electromagnetic wave absorbing performance compared to that in 20 mm thickness.

The minimum reflectivity and bandwidth of the composites are listed in Table 3. Table 3 shows that the frequency corresponding to the minimum reflectivity decreases with the increase of filler content, and this is not influenced by thickness. This is due to the decrease of workability, the increase of macroscopic defects and the increase of water-cement ratio. The absolute value of the minimum reflectivity of the composites in thickness of 10 mm is improved due to the addition of fillers. When the filler content is 3.0% and 6.0%, the maximum absolute value of reflectivity is 89.0% and 143.2% higher than that of composites without fillers. The bandwidth in which the reflectivity is less than -10 dB first increases and then decreases with the increasing filler content. It is increased by 87.5% due to the incorporation of 4.5% GCB composite fillers. The bandwidth in which the reflectivity is less than -15 dB is 0 for the composite without fillers, and it increases to 0.48 as the filler content is 3.0%. The bandwidth in which the reflectivity is less than -10 dB of the composites with 4.5% fillers, i.e. 0.69 vol% graphene, is the same with that of composites with 2.4 vol% CNT/NCB [49]. The bandwidth in which the reflectivity is less than -15 dB of the composites with 3.0% fillers, i.e. 0.47 vol% graphene, also equals to that of composites with 2.4 vol% CNT/NCB [49]. The maximum absolute value of reflectivity of the composites in the thickness of 20 mm has not been improved by the addition of fillers except that of GCB-4.5%. The bandwidth in which the reflectivity is less than -10 dB and -15 dB of GCB-1.5% increases by 13.6% and 56.1% compared with that of cement-based materials without fillers. The maximum absolute values (22.3 dB and 22.1 dB) of reflectivity of GCB-3% in the thickness of 10 mm and 20 mm is larger than that of mortar with 2.5

wt% CB in the thickness of 30 mm (20.3 dB) [32]. The excellent electromagnetic wave self-absorbing property of cement-based materials with GCB composite fillers is mainly due to their good electrical conductivity [55, 56]. Because that cement-based materials with reflectivity less than 10 dB have a very important value both in military and civil use, it can be therefore concluded that cement-based materials with GCB composite fillers is a potential electromagnetic wave absorbing material for infrastructures.

Table 3 Minimum reflectivity and bandwidth of cement-based materials with GCB composite fillers in the frequency of 2-18 GHz

Specimens		Minimum reflectivity (dB) (frequency, GHz)	Bandwidth (reflectivity ≤-10 dB, GHz)	Bandwidth (reflectivity ≤-15 dB, GHz)
In thickness of 10 mm	GCB-0%	-11.8 (16.88)	16.56-17.20	-
	GCB-1.5%	-14.2 (15.60)	15.20-16.00	-
	GCB-3.0%	-22.3 (14.16)	13.84-14.72	14.00-14.48
	GCB-4.5%	-13.9 (7.28)	7.28-7.68 and 12.08-12.88	-
	GCB-6.0%	-28.7 (7.12)	6.88-7.36 and 11.68-12.08	6.96-7.20
	GCB-7.5%	-18.2 (6.48)	2.00-2.24 and 6.16-6.72	6.32-6.56
	GCB-9.0%	-19.6 (2.00)	2.00-2.24 and 5.92-6.40	-
In thickness of 20 mm	GCB-0%	-29.0 (15.10)	11.36-11.92 and 14.32-15.52	14.88-15.28
	GCB-1.5%	-20.9 (14.00)	10.56-11.04, 13.60-14.32 and 16.72-17.52	10.72-10.88, 13.76-14.08 and 17.04-17.20
	GCB-3.0%	-22.1 (9.76)	9.52-10.08, 12.48-13.04 and 15.52-15.92	9.68-9.84 and 12.72-12.80
	GCB-4.5%	-32.6 (3.68)	3.52-3.84, 6.00-6.48 and 8.24-8.80	3.60-3.76 and 6.16-6.24
	GCB-6.0%	-17.9 (3.44)	3.28-3.68 and 5.76-6.08	3.44-3.52
	GCB-7.5%	-12.1 (3.10)	2.96-3.20	-
	GCB-9.0%	-9.8 (2.96)	-	-

4 Conclusions

The electrostatic self-assembled 0D/2D nano carbon materials, i.e. graphene/carbon

black (GCB) composite fillers, can perform synergistic effect to improve the dispersibility of graphene and endow cement-based materials with smart properties without changing the preparation process. Therefore, the smart and multifunctional properties of cement-based materials with GCB composite fillers were investigated and their mechanisms were analyzed. The conclusions are as follows.

The compressive work of cement-based materials with 4.5% GCB composite fillers is 28.6% higher than that of cement-based materials without fillers. Meanwhile, cement-based materials with GCB composite fillers demonstrate low elastic modulus at high compressive strength due to high longitudinal strain of composites. The DC and AC electrical resistivity of cement-based materials are reduced by three and two orders of magnitudes due to the addition of GCB fillers. The overlapped GCB composite fillers play a critical role in the conductivity of the composites. The incorporation of 4.5 wt% GCB composite filler ((i.e. 0.67 vol% graphene) endows cement-based materials with repeatable and stable self-sensing property and the strain sensitivity of composites achieves the maximum value of 19 and 21.2 under cyclic and monotonic compressive loading, respectively. The electromagnetic wave shielding effectiveness of cement-based composites can reach 6.55 dB at the frequency of 9.6 GHz. The minimum reflectivity of the composites in thickness of 10 mm and 20 mm is -28.7 dB and -32.6 dB, respectively. The bandwidth in which the reflectivity is less than -10 dB is increased by 87.5% due to the incorporation of GCB composite fillers.

The cement-based materials with self-assembled 0D/2D nano carbon materials have potential to be used for oil well cementing and smart infrastructures due to excellent properties and simple preparation method.

Acknowledgments

The authors thank the funding supported from the National Science Foundation of China (51908103) and the China Postdoctoral Science Foundation (2019M651116).

References

[1] Yoo D.Y., Banthia N. Impact resistance of fiber-reinforced concrete-A review. Cement Concrete Compos. 2019, 104:103389

[2] Pan Z., Li H., Qiu L., et al. Mechanical properties and microstructure of a graphene oxide-cement composite. Cement Concrete Compos. 2015, 58:140-147.

[3] Materazzi A.L., Ubertini F., Antonella D'Alessandro. Carbon nanotube cement-based transducers for dynamic sensing of strain. Cement Concrete Compos. 2013, 37(1):2-11.

[4] Dong S.F., Han B.G., Ou J.P., et al. Electrically conductive behaviors and mechanisms of short-cut super-fine stainless wire reinforced reactive powder concrete. Cement Concrete Compos. 2016,72:48-65.

[5] Han B.G., Yu X. Ou J.P. Self-sensing concrete in smart structures. Publisher: Elsevier. 2014.

[6] Chiarello M., Zinno R. Electrical conductivity of self-monitoring CFRC. Cement Concrete Comp. 2005, 27(4): 463-469.

[7] Li Z., Ding S.Q., Yu X. Multifunctional cementitious composites modified with nano titanium dioxide: A review. Compos. Part A: App. Sci. Manufac. 2018, 111: 115-137.

[8] Han B.G., Han B.Z., Ou J.P. Experimental study on use of nickel powder-filled Portland cement-based composite for fabrication of piezoresistive sensors with high sensitivity. Sensor. Actuat. A: Phys. 2008, 149(1): 51-55.

[9] Siad H., Lachemi M., Sahmaran M., et al. Advanced engineered cementitious

683 composites with combined self-sensing and self-healing functionalities. Constr. Build.
684 Mater. 2018, (176): 313-322.
685 [10] Parvan M.G., Voicu G., Badanoiu A.I., et al. Self-sensing piezoresistive
686 composites based on cement incorporating low dosage of carbon black used as
687 multifunctional construction materials. Revista de Chimie -Bucharest- Original Edition,
688 2020, 71(5):30-44.
689 [11] Yildirim G., Sarwary M.H., Al-Dahawi A., et al. Piezoresistive behavior of CF-
690 and CNT-based reinforced concrete beams subjected to static flexural loading: shear
691 failure investigation. Constr. Build. Mater. 2018(168): 266-279.
692 [12] Micheli D., Marchetti M., Pastore R., et al. Shielding effectiveness of carbon
693 nanotube reinforced concrete composites by reverberation chamber measurements.
694 Proceedings of the 2015 International Conference on Electromagnetics in Advanced
695 Applications, ICEAA 2015(9):145-148.
696 [13] Jung N. Charge transfer chemical doping of few layer graphenes charge
697 distribution and band gap formation. Nano Lett. 2009, 9(12):4133.
698 [14] Mohamed S., Leung T., Jason F. Enhanced properties of graphene/fly ash
699 geopolymeric composite cement. Cement Concrete Res. 2015, 67: 292-299.
700 [15] Shahil K. M. F., Balandin A. A. Graphene-multilayer graphene nanocomposites
701 as highly efficient thermal interface materials. Nano Lett. 2012, 12(2): 861-867.
702 [16] Babak F., Abolfazl H., Alimorad R., et al. Preparation and mechanical properties
703 of graphene oxide: cement nanocomposites. Sci. World J. 2014, (4):276323.
704 [17] Han B.G., Zheng Q.F., Sun S.W., et al. Enhancing mechanisms of multi-layer
705 graphenes to cementitious composites. Compos. Part A: App. Sci. Manufac. 2017,
706 101:143-150.
707 [18] Han B.G., Ding S.Q., Wang J.L., et al. Nano-engineered cementitious composites:

principles and practices. Springer. 2019.

[19] Jin M., Jiang L., Lu M. Monitoring chloride ion penetration in concrete structure based on the conductivity of graphene/cement composite. Constr. Build. Mater. 2017, 136: 394-404.

[20] Hou D., Yang T., Tang J., et al. Reactive force field Molecular dynamics study on graphene oxide reinforced cement composite: functional groups de-protonation, interfacial bonding and strengthening mechanism. Phys. Chem. Chem. Phys. 2018, 10: 1039.

[21] Rodrigo A.E.S., Guetti P.D.C., Da Luz M.S., et al. Enhanced properties of cement mortars with multilayer graphene nanoparticles. Constr. Build. Mater. 2017, 149(15):378-385.

[22] Xu J., Zhang D. Pressure-sensitive properties of emulsion modified graphene nanoplatelets/cement composites. Cement Concrete Comp. 2017, 84:74-82.

[23] Lu Z., Chen B., Leung C., et al. Aggregation size effect of graphene oxide on its reinforcing efficiency to cement-based materials. Cement Concrete Comp. 2019, 100:85-91.

[24] Liu J., Fu J., Yang Y., et al. Study on dispersion, mechanical and microstructure properties of cement paste incorporating graphene sheets. Constr. Build. Mater. 2019, 199:1-11.

[25] Sam G., Philippe D., Skipper N.T., et al. Understanding the behaviour of graphene oxide in Portland cement paste. Cement Concrete Res. 2018, 111:169-182.

[26] Horszczaruk E., Mijowska E., Kalenczuk Ryszard J., et al. Nanocomposite of cement/graphene oxide-impact on hydration kinetics and Young's modulus. Constr. Build. Mater. 2015, 78:234-242.

[27] Peng H., Ge Y., Cai C.S., et al. Mechanical properties and microstructure of

733 graphene oxide cement-based composites. Constr. Build. Mater. 2019, 194(10):102-
734 109.
735 [28] Singh A.P., Mishra M., Chandra A., et al. Graphene oxide/ferrofluid/cement
736 composites for electromagnetic interference shielding application. Nanotechnology.
737 2011, 22(46):465701
738 [29] Du H., Pang S. D. Dispersion and stability of graphene nanoplatelet in water and
739 its influence on cement composites. Constr. Build. Mater. 2018, 167:403-413.
740 [30] Jing G., Ye Z.M., Lu X., et al. Effect of graphene nanoplatelets on hydration
741 behaviour of Portland cement by thermal analysis. Adv. Cem. Res. 2017, 29(2):63-70.
742 [31] Zheng Q., Han B., Cui X., et al. Graphene-engineered cementitious composites:
743 small makes a big impact. Nanomater. Nanotechno. 2016, 7:119-136.
744 [32] Dai Y., Sun M., Liu C., et al. Electromagnetic wave absorbing characteristics of
745 carbon black cement-based composites. Cement Concrete Comp. 2010, 32(7):508-513.
746 [33] Monteiro A.O., Cachim P.B., Costa P.M.F.J., et al. Self-sensing piezoresistive
747 cement composite loaded with carbon black particles. Cement Concrete Comp. 2019,
748 8159-65.
749 [34] Monteiro, A.O., Loredo A., Costa P.M.F.J., et al., 2017. A pressure-sensitive
750 carbon black cement composite for traffic monitoring. Constr. Build. Mater. 2017,
751 154:1079-1086.
752 [35] Han B.G., Ding S. Q., Yu X. Intrinsic self-sensing concrete and structures: A
753 review. Measurement. 2015, 59:110-128.
754 [36] Prvan M.G., Voicu G., Bdnoiu A.I. Study of hydration and hardening processes of
755 self-sensing cement-based materials with carbon black content. J. Therm. Anal.
756 Calorime. 2020(139): 807-815.
757 [37] Das E., Kaplan B.Y., Gursel S.A., et al. Graphene nanoplatelets-carbon black

758 hybrids as an efficient catalyst support for Pt nanoparticles for polymer electrolyte
759 membrane fuel cells. Renew. Energy. 2019, 139:1099-1110.
760 [38] Qiu X., Zhao X., Liu F., et al. Surfactant-free carbon black@graphene conductive
761 ink for flexible electronics. J. Mater. Sci. 2019, 54(16):11157-11167.
762 [39] Collins F., Lambert F., Duan W.H. The influence of admixtures on the dispersion,
763 workability, and strength of carbon nanotube–OPC paste mixtures. Cement Concrete
764 Compos. 2012;34(9):1067-74.
765 [40] Öztürk O., Sultan KeskinÜ., Sahmaran M. Self-sensing fiber reinforced cement
766 mortars for the monitoring of critical and transport infrastructures. EGU General
767 Assembly Conference Abstracts, 2018: 2000.
768 [41] Öztürk O., Yıldırım G., Keskin U.S., et al. Nano-tailored multi-functional
769 cementitious composites. Compo. Part B: Eng. 2019:107670.
770 [42] Han B. G., Zhang L.Q., Ou J. P. Smart and multifunctional concrete toward
771 sustainable infrastructures. Springer. 2017.
772 [43] Li L.W., Dong S.F., Dong X.F. Electromagnetic wave shielding/absorption
773 performances of cementitious composites incorporating carbon nanotube metamaterial
774 with helical chirality. J. Compos. Mater. 2020, 54(25): 3857-3870.
775 [44] Pastore R., Micheli D., Vricella A., et al. Advanced concrete materials for EMI
776 reduction in protected environment and IEMI threats suppression[C]//IEEE
777 International Conference on Environment & Electrical Engineering. IEEE, 2015: 2011-
778 2016.
779 [45] Lu S., Wang X., Meng Z., et al. The mechanical properties, microstructures and
780 mechanism of carbon nanotube-reinforced oil well cement-based nanocomposites. RSC
781 Advances. 2019, 9(46):26691-26702.
782 [46] Lavagna L., Musso S., Ferro G., et al. Cement-based composites containing

783 functionalized carbon fibers. Cement Concrete Compos. 2018, 88: 165-171.
784 [47] Musso S., Tulliani J.M., Ferro G., et al. Influence of carbon nanotubes structure
785 on the mechanical behavior of cement composites. Compos. Sci. Technol. 2009,
786 69:1985-1990
787 [48] Han B., Zhang L., Zeng S., et al. Nano-core effect in nano-engineered cementitious
788 composites. Compos. Part A: App. Sci. Manufac. 2017, 95:100-109.
789 [49] Han B.G., Zhang L.Q., Sun S.F., et al. Electrostatic self-assembly carbon
790 nanotube/nano carbon black composite fillers reinforced cement-based materials with
791 multifunctionality. Compos. Part A: App. Sci. Manufac.2015,79:103-115.
792 [50] Yoo D. Y., You. I., Lee S.J. Electrical properties of cement-based composites with
793 carbon nanotubes, graphene, and graphite nanofibers. Sensors, 2017, 17(5):1064-1076.
794 [51] Han B.G., Ou J.P. Embedded piezoresistive cement-based stress/strain sensor.
795 Sensor. Actuat. A: Phys. 2007, 138(2): 294-298.
796 [52] Ou J.P., Han B.G. Piezoresistive cement-based strain sensors and self-sensing
797 concrete components. J. Intel. Mat. Syst. Str. 2009, 20 (3):329-336.
798 [53] Dong S.F., Zhou D.C., Li Z., et al. Super-fine stainless wires enabled
799 multifunctional and smart reactive powder concrete. Smart Mater. Struct. 2019, 28(12):
800 125009.
801 [54] Mason T.O., Campo M.A., Hixson A.D., et al. Impedance spectroscopy of fiber-
802 reinforced cement composites. Cement Concrete Comp. 2002, 24(5):457-465.
803 [55] Lee S., Kang D., Oh I.K. Multilayered graphene-carbon nanotube-iron oxide three-
804 dimensional heterostructure for flexible electromagnetic interference shielding film.
805 Carbon. 2017, 111:248-57.
806 [56] Che R., Peng L.M. Duan X.F. et al. Microwave absorption enhancement and
807 complex permittivity and permeability of Fe encapsulated within carbon nanotubes.

808 Adv. Mater. 2004, 16(5):401-405.